J Paleolimnol
https://doi.org/10.1007/s10933-020-00114-4

ORIGINAL PAPER

Resolving combined influences of inflow and evaporation on western Greenland lake water isotopes to inform paleoclimate inferences

A. A. Cluett · E. K. Thomas

Received: 10 June 2019 / Accepted: 18 January 2020

Abstract Stable isotopes of oxygen ($\delta^{18}O$) and hydrogen ($\delta^{2}H$) in precipitation are widely employed tracers of the global hydrologic cycle, and are frequently inferred from lake-water-derived proxies in sediments of high-latitude lakes. Lake-water isotope proxies archive precipitation $\delta^{18}O$ and $\delta^{2}H$ values, modulated by lake hydrological processes, which may be functionally classified into processes that affect source water isotope values (i.e. inflow $\delta^{18}O$ and $\delta^{2}H$) and catchment-integrated evaporation. Respectively, these controls form the basis of interpretations of precipitation isotope and effective precipitation signals from lake-water isotope proxy records. Conventionally, a single control on lake water isotope variability is assumed for a given record. Yet sensitivity to these controls depends on regional hydroclimate and local hydrology, which may change through time. We quantified the relative impacts of variations in inflow $\delta^{18}O$ and evaporative ^{18}O enrichment on lake water $\delta^{18}O$ in response to spatially variable aridity, using measurements of lake water $\delta^{2}H$ and $\delta^{18}O$ from 140 western Greenland lakes located between the Labrador Sea and western Greenland Ice Sheet margin. We calculated source water $\delta^{18}O$ of lake waters (δI) using a recently developed Bayesian method and quantified evaporation-to-inflow ratios (E/I) using a modified Craig-Gordon model. δI varied by 11.1‰ across the study region, superimposed by evaporative ^{18}O enrichment of up to 20.0‰ and E/I ranging from nearly no evaporative loss ($E/I < 0.10$) to desiccation ($E/I > 1$). Lakes can be broadly classified as predominantly sensitive to inflow or evaporation, corresponding to their location along the aridity gradient, and there are significant trends in both δI and E/I across the study area. Substantial local variability in δI and E/I suggests catchment hydrology determines the sensitivity of δI and E/I to changes in aridity, and implies that hydrological end-member lakes within a small region may provide complementary records of seasonal precipitation isotope values and ice-free-season evaporation. Deconvolving modern controls on lake water isotope values provides essential support for quantitative and seasonal paleoclimate inferences from paleolimnological isotope data, which will improve constraints on the long-term variability of the Arctic hydrologic cycle.

Keywords Lake water isotopes · Precipitation isotopes · Arctic · Hydroclimate · Effective precipitation · Proxy interpretation

Electronic supplementary material The online version of this article (https://doi.org/10.1007/s10933-020-00114-4) contains supplementary material, which is available to authorized users.

A. A. Cluett (✉) · E. K. Thomas
University at Buffalo, State University of New York, Buffalo, NY 14260, USA
e-mail: aacluett@buffalo.edu

Published online: 05 February 2020

Introduction

The hydrologic cycle in the Arctic is intricately linked to the cryosphere and the global climate system, and is projected to change profoundly in response to anthropogenic warming (Serreze et al. 2006). Annual Arctic precipitation may increase by up to 50% within the century in response to increasing freshwater fluxes between the atmosphere, land, and oceans (Rawlins et al. 2010; Bintanja and Selten 2014). Yet ramifications of such a precipitation increase for ice sheet mass balance, terrestrial hydrology, ecosystems, and ocean circulation will depend on both the magnitude and seasonality of future changes (Bring et al. 2016). The mechanisms predicted to drive precipitation changes are associated with contrasting seasonality, with increases in winter precipitation driven by enhanced local evaporation and increases in summer precipitation driven by strengthened remote moisture transport (Bintanja and Selten 2014). Understanding the relative importance of these seasonal mechanisms to future changes is limited by a lack of constraints on long-term seasonal moisture variability in the Arctic, a consequence of the scarcity of qualitative records and absence of quantitative records (Linderholm et al. 2018).

The stable isotope compositions of oxygen and hydrogen ($\delta^{18}O$ and $\delta^{2}H$) in precipitation are powerful tracers of hydroclimate, as they are affected by transport and fractionation processes within the global hydrologic cycle (Dansgaard 1964; Gat 1996). Direct measurement of precipitation $\delta^{18}O$ and $\delta^{2}H$ in ice cores has produced paleoclimate records from glaciated regions (Andersen et al 2004; Dansgaard et al 1993). Additionally, proxy data for past precipitation $\delta^{18}O$ and $\delta^{2}H$ values are archived indirectly in Holocene-age Arctic lake sediments, the most widespread archives of such information (Leng and Marshall 2004; Sundqvist et al. 2014).

A recent synthesis of Holocene proxy data from the Arctic included 14 lake water $\delta^{18}O$ or $\delta^{2}H$ records, measured in calcite, cellulose, diatoms, and leaf wax biomarkers (Sundqvist et al. 2014). Most of these records (n = 8) were originally interpreted as relative mean annual effective precipitation (P-E), with the remaining records interpreted as reflecting mean annual precipitation isotope values. With continued growth in the application of lake water isotope proxies, interpretations of Arctic records have broadened to include relative precipitation seasonality and summer-biased precipitation isotopes (Arppe et al. 2017; Balascio et al. 2018; Lasher et al. 2017; Lasher and Axford 2019; Thomas et al. 2016, 2018). Although all of these Arctic lake water isotope proxy records may be classified as 'hydroclimate-sensitive,' such a classification comprises a broad range of interpretations, which may be divided into those that reflect precipitation isotopes and those that reflect P-E balance.

Interpretations of lake water proxy $\delta^{18}O$ and $\delta^{2}H$ in sediment cores are often supported by local measurements of modern lake water and/or precipitation $\delta^{18}O$ and $\delta^{2}H$ (Anderson et al. 2005; Balascio et al. 2013; Lasher and Axford 2019; Thomas et al. 2016). Modern lake water surveys from the Arctic and sub-Arctic demonstrate that lakes may exhibit wide ranges of $\delta^{18}O$ and $\delta^{2}H$, despite receiving similar annual precipitation input (Gibson and Edwards 2002; Jonsson et al. 2009; Leng and Anderson 2003). Deviation of lake water $\delta^{18}O$ and $\delta^{2}H$ from annual precipitation values has been linked to differences in water residence time and hydrologic connectivity, which cause differences in apparent inflow isotope values (Gibson et al. 2002). Moreover, observations of regional lake water isotopic variability may extend beyond the range of precipitation isotopic variability, implicating modification by evaporation (Gibson and Edwards 2002; Leng and Anderson 2003). Simply, processes that drive lake water variability may be divided into those that affect inflow $\delta^{18}O$ and $\delta^{2}H$ and those that impart evaporative ^{18}O and ^{2}H enrichment, analogous to paleoclimate interpretations of precipitation isotopes and P-E.

The Kangerlussuaq region spans the widest ice-free corridor of Greenland, displaying a transition from maritime climate along the coast of the northern Labrador Sea to continental climate towards the Greenland Ice Sheet margin. Several lakes from the region have yielded paleolimnological records that contextualize Holocene ice sheet retreat and document local ecological changes following deglaciation (Anderson and Leng 2004; Leng et al. 2012). Kangerlussuaq is the focus of a substantial body of work in modern isotope hydrology. The region has served as the setting of multi-year surveys of lake water isotopes (Kopec et al. 2018; Leng and Anderson 2003) and detailed work on water isotope systematics of atmospheric moisture, lake water evaporation, and leaf

water evaporation (Kopec et al. 2014; Feng et al. 2016; Bush et al. 2017). Our work builds upon two prior lake water studies from the region, which combined, now include 10 years of data across two decades (Kopec et al. 2018; Leng and Anderson 2003).

Earliest analysis of modern lake water isotopes in the Kangerlussuaq region characterized spatial variation in lake water $\delta^{18}O$ and $\delta^{2}H$ between the coast and the ice sheet (Leng and Anderson 2003). Whereas inland, hydrologically closed-basin lakes demonstrated sensitivity to evaporative ^{18}O and ^{2}H enrichment in response to variations in interannual precipitation amount, coastal lakes maintained $\delta^{18}O$ and $\delta^{2}H$ near mean annual precipitation values. The identification of evaporation as a dominant local control informed the interpretation of Holocene carbonate $\delta^{18}O$ records produced from two inland lakes (Anderson and Leng 2004). Strongly negative P-E in the middle Holocene was interpreted from ^{18}O enrichment in carbonate $\delta^{18}O$ of both lakes. Despite periods of broad agreement between the two records, substantial discrepancies exist and interpretations are limited to relative trends, with a more refined understanding limited, in part, by substantial age model uncertainty. A subsequent study by Kopec et al. (2018) reported several years of lake water $\delta^{18}O$ and $\delta^{2}H$ measurements from an overlapping subset of inland lakes, and employed principal components analysis (PCA) to document interannual variations in regional-scale isotope enrichment. Variability along the first PC related to lake water evaporative enrichment, with correlation observed between the first PC slope and regional atmospheric circulation. PC-inferred isotope enrichment of individual lakes, however, was determined to have been too complex to extract a specific hydroclimate signal. Yet paleoclimate studies typically rely on reconstruction of $\delta^{18}O$ or $\delta^{2}H$ from just one or two lakes. A gap remains in our understanding of the magnitude of influence of the primary processes that determine $\delta^{18}O$ and $\delta^{2}H$ values in a single lake within the Kangerlussuaq region.

We report measurements of $\delta^{18}O$ and $\delta^{2}H$ from 140 lakes near Kangerlussuaq Fjord sampled during summers of 2016 and 2018. The data revealed additional constraints on the spatial and inter-annual variability of precipitation- and glacial-meltwater-fed lake water isotopic compositions in the region. Sampled lakes were distributed along a transect between the coast and ice sheet, providing a gradient that included precipitation-dominated coastal lakes and evapo-concentrated inland lakes. Our publicly available dataset (www.waterisotopes.org, project ID 00256) contributes to a growing body of lake water isotope data from this region.

To determine the sensitivity of lake water isotopes to changes in precipitation isotopes and P-E across different hydroclimate conditions, we calculated source water $\delta^{18}O$ of lake waters (δI) using a recently developed Bayesian source water attribution method and quantified evaporation-to-inflow ratios (E/I) using a modified Craig-Gordon model (Bowen et al. 2018; Gibson et al. 2016). Inflow and lake water evaporation independently drive variations of $> 10‰$ in lake water $\delta^{18}O$ within the study region, and provide support for the observation of Leng and Anderson (2003) that the predominant hydrological control on isotope values in lakes shifts from inflow to evaporation between the coast and the ice margin. Although the isotope values of most lakes demonstrate sensitivity to both hydrological processes, we propose that the presence of some lakes with strongly evaporation-sensitive and others with inflow-sensitive isotopic compositions on local scales suggests that hydrologic-endmember lakes within this and other Arctic regions can provide complementary paleoclimate reconstructions, reflecting either P-E balance or seasonally-specific precipitation isotopes.

Study region

The study area spans the most expansive ice-free margin of Greenland, approximately 180 km between the western margin of the Greenland Ice Sheet and the Labrador Sea, from 66.6° N to 67.5° N (Fig. 1). The ice sheet retreated from the coast ca. 10,000 years BP and shaped the region's underlying low-relief granodioritic gneiss bedrock, nearing its present margin ca. 2000 cal years BP (Lesnek et al. 2020). Kangerlussuaq Fjord, located in the central study area, is one of several fjords that dissect the region and drain ice sheet meltwater into Davis Strait. Lakes cover approximately 20% of the surface in a combination of large fjord-lake systems, small glacial-scoured basins, and shallow meltwater pools (Anderson et al. 1999).

Three stations within the study region record hourly temperature and relative humidity, documenting a strong hydroclimate gradient between the coast and ice sheet (Cappelen 2017; Smeets et al. 2018) (Fig. 2).

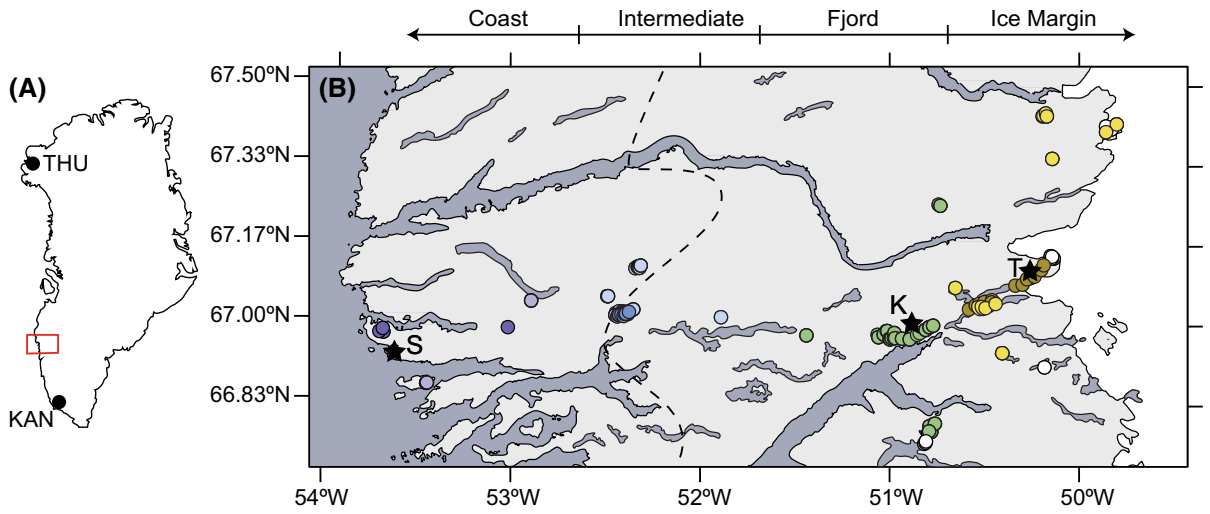

Fig. 1 **a** Map of Greenland with study area in red box, and Thule (THU) and Kangilinnguit (KAN) GNIP stations (IAEA 2018). **b** Study area with sampled proglacial lakes (white) and non-glacial lakes, with point color corresponding to sub-region and year as in Fig. 3. Locations of Kangerlussuaq (K), Sisimiut (S), and Two Boat Lake (T) weather stations (stars) are indicated. The approximate boundary in effective precipitation (P-E) as identified by Hasholt and Søgaard (1978) is denoted by a dashed line, with positive P-E to the west and negative P-E to the east

Proximity to Davis Strait stabilizes temperatures along the coast, where temperature seasonality is muted relative to locations near the ice margin (Fig. 2a). Easterly katabatic winds drive cold, dry, ^{18}O- and ^{2}H-depleted atmospheric moisture from the ice sheet towards the coast, whereas sea breezes bring warmer, ^{18}O- and ^{2}H-enriched moisture inland (Kopec et al. 2014). Local evaporation of lake water and fjords drives small-scale variation in relative humidity and atmosphere water vapor isotope compositions (Feng et al. 2016). A preliminary hydrological survey by Hasholt and Søgaard (1978) mapped a boundary between positive and negative moisture balance (P-E) near 52° W (Fig. 1). Dwarf-shrub tundra communities vary from moist heath vegetation near the coast to sparse vegetation inland, reflecting decreased moisture availability with increasing distance from the coast (Leng and Anderson 2003). Significant differences in precipitation amount between coastal and inland sites are observed in fall and winter (Fig. 2e), and a large difference in relative humidity between sites ($\sim$ 25%), occurs in summer (Fig. 2b). Summer 2018 was more humid than summer 2016 by an average of 5% within the Fjord and Ice Margin Regions (NOAA 2018). Several precipitation events occurred during the period of 2018 sampling, but none occurred during the period of 2016 sampling.

Lakes in the region are ice-free only June through August or September (Anderson and Brodersen 2001). Continuous permafrost limits subsurface hydrologic flow to a thin active layer that ranges from 0.15 to 5 m depth between Kangerlussuaq and the ice sheet, and geochemical evidence suggests that groundwater-surface water interactions have little influence on lake chemistry (Van Tatenhove and Olesen 1994; Johansson et al. 2015; Henkemans et al. 2018). Thus, permafrost and sub-surface inflow are likely minor sources of inflow to lakes in this region. Surface inflow is sourced from a combination of precipitation and glacial meltwater. Proglacial lakes that receive inflow from glacial meltwater can be distinguished by the presence of glacial flour in the water column. We refer to lakes that receive only precipitation input as non-glacial. Sampled non-glacial lakes were divided into four equal longitudinal zones, each 0.92° wide, which represent Coastal, Intermediate, Fjord, and Ice Margin sub-regions (Fig. 1).

Regional isotopic setting

The global average relationship between δ^{18}O and δ^{2}H of precipitation is described by the Global Meteoric Water Line (GMWL), $\delta^{2}H = 8*\delta^{18}O + 10$ (Craig 1961) (Fig. 3a). The isotopic composition of

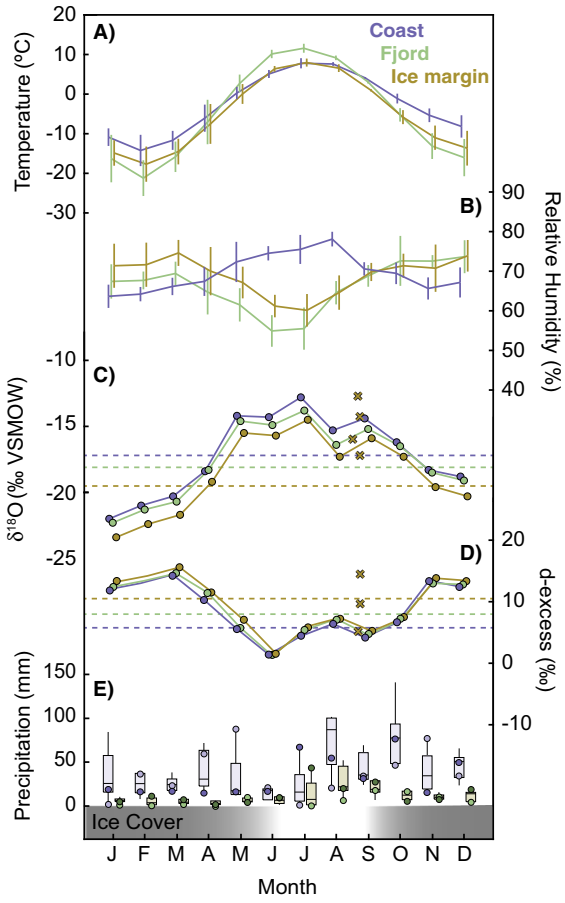

Fig. 2 Mean monthly temperature (**a**) and relative humidity (**b**) from 2014 to 2018 for Sisimiut/Coast (blue), Kangerlussuaq/Fjord (green), and Two Boat Lake Catchment/Ice Margin (yellow) (Cappelen 2017; Smeets et al. 2018). Vertical bars represent one standard deviation from the mean. **c** OIPC-interpolated monthly precipitation $\delta^{18}O$ at meteorological station locations (Bowen 2018). Dashed lines represent amount-weighted mean annual precipitation $\delta^{18}O$ at each site. Yellow Xs denote $\delta^{18}O$ of precipitation events sampled in the TBL catchment during August 2014 (Lindborg et al. 2016). **d** OIPC monthly precipitation d-excess at meteorological station locations and mean annual precipitation d-excess (dashed lines) (Bowen 2018). Yellow Xs denote d-excess of precipitation events sampled in the TBL catchment during August 2014 (Lindborg et al. 2016). **e** Monthly accumulated precipitation for Sisimiut and Kangerlussuaq from 2014 to 2018 (NOAA 2018). Dots indicate values for 2016 (light) and 2018 (dark). (Color figure online)

precipitation may deviate from the GMWL because of local moisture source and transport conditions, resulting in a distinct local meteoric water line (LMWL) (Gat 2000). Two coastal sites in western Greenland have been monitored as part of the Global Network of Isotopes in Precipitation (GNIP): Thule (76.52° N, 68.83° W), approximately 1300 km north of the study area and Kangilinnguit (61.22° N, 48.12° W), approximately 700 km south of the study area (IAEA/WMO 2018). These sites yield LMWLs with the equations $\delta^2H = 7.33*\delta^{18}O - 7.14$ and $\delta^2H = 6.42*\delta^{18}O - 15.43$, respectively, with the Thule LMWL ^{18}O- and ^2H-depleted relative to the Kangilinnguit LMWL. Summer rain (n = 4) and spring snowpack (n = 6) sampled within the study area (Two Boat Lake Catchment (TBL): 67.13° N, 50.18° W) produced a LMWL with the equation $\delta^2H = 6.27*\delta^{18}O - 19.22$, overlapping the ranges of the Thule and Kangilinnguit LMWLs (Lindborg et al. 2016) (Fig. 3a). Comparison of rain and snowpack LMWL end-members indicates substantial seasonality in precipitation $\delta^{18}O$ and δ^2H in the Kangerlussuaq region, supported by Online Isotopes in Precipitation Calculator (OIPC)-interpolated monthly precipitation, which demonstrates strong seasonal cycles in precipitation $\delta^{18}O$ and d-excess (Bowen 2018) (Fig. 2c, d).

Materials and methods

Sampling and analytical methods

Lake water samples were collected in the summers of 2016 and 2018, with partial overlap in the lakes sampled. Single samples were collected from 89 lakes during a 3-week period in July and August 2016, and 63 lakes within a 3-week period in July and August 2018 (Fig. 1). No relationship is observed between sampling date and measured $\delta^{18}O$ or δ^2H (Electronic Supplementary Material [ESM] Figs. S1 and S2). Samples were, however, collected near the end of the ice-free season, and therefore likely represent maximum seasonal evaporative ^{18}O enrichment.

Near-surface lake water samples were collected from the shoreline or from a boat in each lake, stored in 4-mL glass vials or 50-mL centrifuge tubes with no headspace, and sealed with Parafilm to prevent evaporation during transport. Samples were collected approximately 5 to 10 cm below the lake surface and should not contain evaporatively ^{18}O- and ^2H-enriched water from near the water-air interface (Horita et al. 2008). Bottom-water samples were collected from above the sediment-water interface of cores

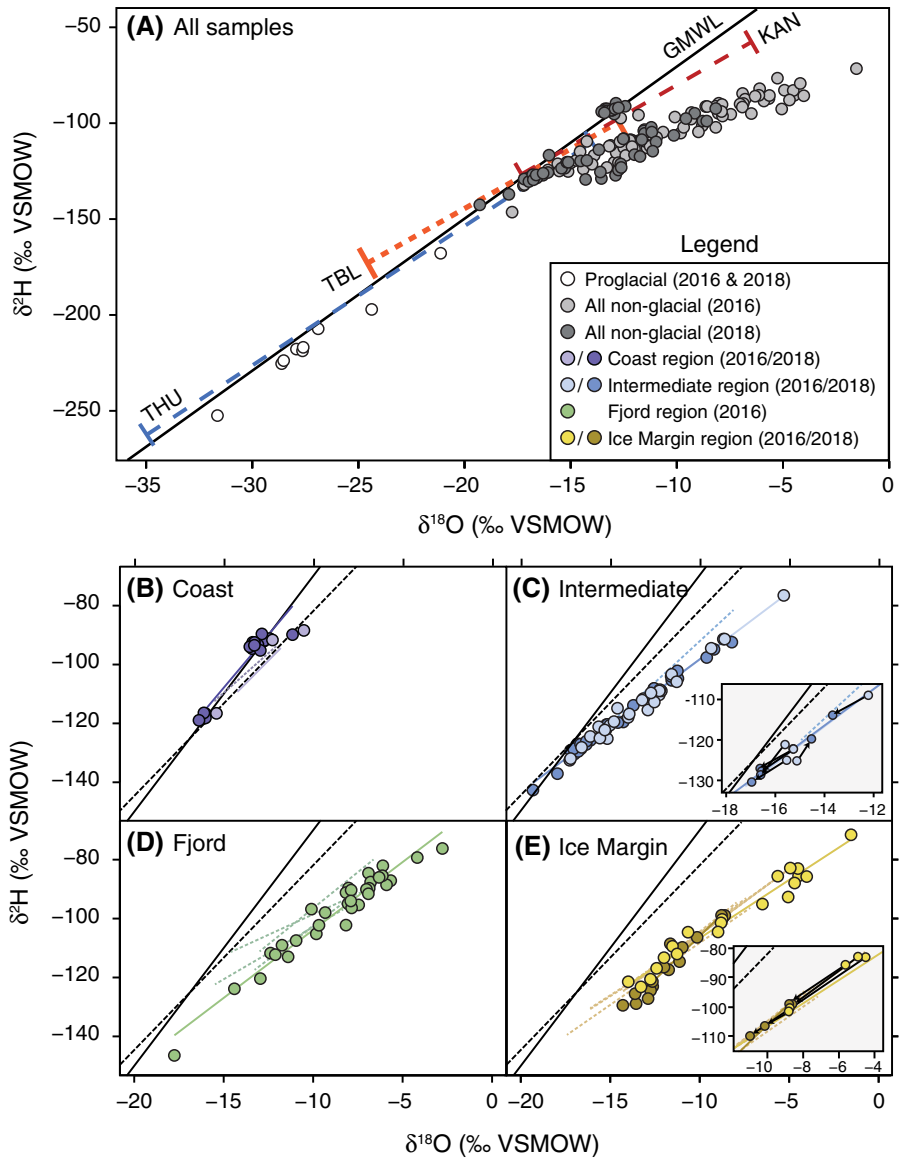

Fig. 3 **a** $\delta^{18}O$ versus $\delta^{2}H$ for all lake water samples including non-glacial lake samples from 2016 (light gray), non-glacial lake samples from 2018 (dark gray), and proglacial lake samples from both years (white), plotted against the global meteoric water line (GMWL, $\delta^{2}H = 8*\delta^{18}O + 10$) and local meteoric water lines (LMWLs) from Kangilinnguit (KAN, $\delta^{2}H = 6.42*\delta^{18}O - 15.43$), Two Boat Lake Catchment (TBL, $\delta^{2}H = 6.27*\delta^{18}O - 19.22$) and Thule (THU, $\delta^{2}H = 7.33*\delta^{18}O - 7.14$). $\delta^{18}O$ versus $\delta^{2}H$ for non-glacial samples from the Coast sub-region (**a**), Intermediate sub-region (**b**), Fjord sub-region (**c**), and Ice Margin sub-region (**d**). Local evaporation lines (LELs) are included in panels B–E from samples from this study (solid) and previous studies (dashed). Inset panels for the Intermediate and Ice Margin sub-regions show the relative positions in $\delta^{18}O$–$\delta^{2}H$ space of lakes sampled in both years

taken from 8 lakes in 2016. Prior to analysis, water samples were filtered using 0.2-µm PTFE filters.

For samples collected in 2016, $\delta^{18}O$ and $\delta^{2}H$ were measured on a Picarro L2130-i Water Isotope Analyzer at the University of Massachusetts-Amherst Stable Isotope Laboratory. Reported analytical uncertainties were 0.08‰ and 0.51‰ for $\delta^{18}O$ and $\delta^{2}H$, respectively, based on the standard deviation of replicate measurements. A correction was applied to account for long-term instrument drift, with uncertainties of 0.15‰ and 1.0‰ for $\delta^{18}O$ and $\delta^{2}H$, respectively.

For samples collected in 2018, $\delta^{18}O$ and $\delta^{2}H$ were measured on a Picarro L2130-i at the University at Buffalo Organic and Stable Isotope Biogeochemistry Laboratory. Samples were measured five times, with the first two measurements discarded. Reported values are the mean of the last three measurements, calibrated to the VSMOW scale using a suite of secondary standards prepared in-house. The secondary standards span a range of − 40.1 to + 12.41‰ $\delta^{18}O$ and − 321.2 to 21.4‰ $\delta^{2}H$, as calibrated by primary standards (GISP, VSMOW2, and SLAP2) from the International Atomic Energy Agency (IAEA). A

memory correction was determined and applied for each sequence (van Geldern and Barth 2012). Average standard deviations of replicate measurements were 0.02‰ and 0.08‰ for $\delta^{18}O$ and $\delta^{2}H$, respectively.

Isotope ratios are reported in per mil (‰) relative to Vienna Standard Mean Ocean Water (VSMOW), where $\delta = 1000*((R_{sample}/R_{VSMOW}) - 1)$ and R is $^{18}O/^{16}O$ or $^{2}H/^{1}H$. Deuterium-excess (d-excess) was calculated as d-excess = $\delta^{2}H - 8*\delta^{18}O$ (Dansgaard 1964). $\delta^{18}O$ and $\delta^{2}H$ strongly correlate for proglacial ($R^2 = 0.99$) and non-glacial ($R^2 = 0.91$) lake samples. Hereafter, we primarily discuss $\delta^{18}O$ and d-excess, and trends in $\delta^{2}H$ can be assumed to follow $\delta^{18}O$.

Inference of inflow $\delta^{18}O$

In $\delta^{18}O$–$\delta^{2}H$ space, a precipitation-fed lake undergoing evaporation will evolve along a local evaporation line (LEL), deviating from its starting isotopic composition along the MWL (Gat 1996). Thus, $\delta^{18}O$ and $\delta^{2}H$ of source water entering an evapo-concentrated lake may be calculated from the LEL-MWL intersection, given the MWL and LEL slopes (Gonfiantini 1986). As predicted by the Craig-Gordon model, an LEL slope depends on the conditions that influence kinetic fractionation during evaporation, primarily relative humidity and atmospheric vapor $\delta^{18}O$ and $\delta^{2}H$ (δA) (Craig and Gordon 1965). Regional LELs are commonly estimated as linear regressions of $\delta^{18}O$ and $\delta^{2}H$ measurements from several lake waters within a region (Clark and Fritz 1997). This approach assumes that all lake waters within a region begin with the same isotopic composition, and all variation in lake water isotopic compositions is a consequence of evaporative ^{18}O and ^{2}H enrichment (Bowen et al. 2018). These assumptions, however, are rarely valid among lakes in a region, especially where strongly seasonal precipitation $\delta^{18}O$ and $\delta^{2}H$ values drive variations in inflow $\delta^{18}O$ and $\delta^{2}H$ throughout the year. Consequently, source water $\delta^{18}O$ and $\delta^{2}H$ values and their uncertainties, inferred from the regional LEL-MWL intersection, may be erroneous, in this study region and throughout much of the Arctic.

We applied a Bayesian 'MWL source implementation' method developed by Bowen et al. (2018) to estimate the isotope composition of source waters to evapo-concentrated, non-glacial lakes. The method incorporates uncertainty in the MWL and LEL, providing a more rigorous estimate of source water uncertainty. Briefly, a prior distribution of possible source water $\delta^{18}O$ and $\delta^{2}H$ values is generated from an MWL. The relative conditional probabilities of iterative draws from the prior distribution are calculated with the following steps: (1) a source water value is drawn from the prior distribution, (2) the slope of the LEL between the observed lake water value and drawn source water value is calculated, (3) the conditional probability of this hypothesized LEL slope is calculated given a probability density distribution defined as the true LEL slope. Source water draws are saved in proportion to their conditional probability as a posterior distribution from which median source water $\delta^{18}O$ and uncertainty intervals are calculated.

To apply the 'MWL source implementation' method, we supply an MWL and confidence interval, an estimated LEL and confidence interval, lake water $\delta^{18}O$ and $\delta^{2}H$ with uncertainty and covariance, and the number of iterations. Given the similarity between the LMWL and the GMWL and the small number of samples on which the LMWL is based, we employ the GMWL. We supply mean LEL slopes as calculated for three sub-regions defined across the study area across all years for which there is published data (excluding the anomalously steep 2018 Ice Margin slope), and a standard confidence interval of 0.5. Average LEL slopes are 4.39 for the Ice Margin sub-region, 3.94 for the Fjord sub-region, and 4.53 for the Intermediate sub-region. We acknowledge that mean LEL slopes likely reflect maximum values and may underestimate source water values (Bowen et al. 2018). Even so, average LEL slopes ($\sim$ 4) agree with theoretical ice-free LEL slopes as modeled in Gibson et al. (2008), meaning that these are likely a robust starting estimate. Lake water input $\delta^{18}O$ and $\delta^{2}H$ are measured sample values with analytical error, and covariance prescribed as 0.95. 10,000 iterations are employed per lake. Median posterior values are reported with the 90% confidence interval.

The Bayesian method was applied to all sampled non-glacial lakes except those in the Coast sub-region, which are not measurably affected by evaporative ^{18}O enrichment and are assumed to have values equivalent to unevaporated inflow values. We refer to assumed inflow from the Coast sub-region lakes and Bayesian modeled inflow for all other sub-regions as inferred inflow $\delta^{18}O$ (δI).

Quantification of evaporation ^{18}O enrichment and E/I

A modified Craig-Gordon model was employed to calculate the fraction of evaporative loss relative to inflow (E/I) for all evapo-concentrated non-glacial lakes, as formulated in Gibson et al. (2016). Although shallow Arctic lakes are characterized by transient hydrological conditions, steady-state models may be used to legitimately estimate long-term (i.e. approximately annual) evaporation and outflow in Arctic regions (Gibson 2002).

Assuming hydrological steady-state, the water mass balance and isotope mass balance of an evaporating lake may be described by:

$$I_L = Q_L + E_L \tag{1}$$

$$I_L \delta I = Q_L \delta Q + E_L \delta E \tag{2}$$

where I_L is combined surface and subsurface inflow flux, Q_L is combined surface and subsurface outflow flux, and E_L is lake evaporation flux. δI, δQ, and δE are the $\delta^{18}O$ or δ^2H values of inflow, outflow, and evaporative flux, respectively.

Assuming δQ is equivalent to lake water $\delta^{18}O$ or δ^2H (δL) and substituting $Q_L = I_L - E_L$, the ratio of inflow to outflow is provided by:

$$\frac{E_L}{I_L} = \frac{\delta I - \delta L}{\delta E - \delta L} \tag{3}$$

As implemented here, δL is measured lake water $\delta^{18}O$ or δ^2H and δI is inferred inflow $\delta^{18}O$ or δ^2H. δE is calculated following the standard approach developed in the Craig-Gordon model, assuming negligible resistance to mixing in the liquid phase (Gat 1995).

$$\delta E = \frac{\alpha^* \delta L - h * \delta A - \varepsilon}{1 - h + 10^{-3}\varepsilon_K} \tag{4}$$

α* is the equilibrium liquid-vapor isotope fractionation ($\alpha^* = 1 + \varepsilon^*$), h is the atmospheric relative humidity presented in decimal form, δA is $\delta^{18}O$ or δ^2H of atmospheric moisture, and ε is the total isotopic separation factor, comprised of equilibrium (ε*) and kinetic (ε_K) components ($\varepsilon = \varepsilon^* + \varepsilon_K$). Gat (1995) determined ε_K empirically according to Eq. 5, with a dependence on relative humidity with a kinetic fractionation constant (C_K) of 14.2‰ for $\delta^{18}O$ or 12.5‰ for δ^2H (Gonfiantini 1986).

$$\varepsilon_K = (1 - h) * C_K \tag{5}$$

ε* has been determined empirically by Horita and Wesolowski (1994), according to Eq. 6 for $\delta^{18}O$ and Eq. 7 for δ^2H, where T is the interface temperature (K), here assumed to be average summer air temperature. δA is assumed to be in equilibrium with ice-free-season precipitation $\delta^{18}O$ or δ^2H, calculated as the amount-weighted average of the monthly OIPC estimates retrieved at each lake coordinate (Bowen 2018). Ice-free-season relative humidity and temperature for 2016 and 2018 were retrieved from the Sisimiut, Kangerlussuaq, and TBL meteorological stations (NOAA 2018; Smeets et al. 2018) (Table S1). Values from the closest meteorological station were applied for each lake.

$$\begin{aligned}\varepsilon^* &\approx 10^3 \ln \alpha(^{18}O) \\ &= -7.685 + 6.7123\left(\frac{10^3}{T}\right) - 1.6664\left(\frac{10^6}{T^2}\right) \\ &\quad + 0.35041\left(\frac{10^9}{T^3}\right)\end{aligned} \tag{6}$$

$$\begin{aligned}\varepsilon^* &\approx 10^3 \ln \alpha(^{2}H) \\ &= 1158.8 * \left(\frac{T^3}{10^9}\right) - 1620.1\left(\frac{T^2}{10^{-6}}\right) \\ &\quad + 794.84\left(\frac{T}{10^3}\right) - 161.04 + 2.9992\left(\frac{10^9}{T^3}\right)\end{aligned} \tag{7}$$

Given that all Coast sub-region samples fall along MWLs (Fig. 3b) and the assumption that lake water $\delta^{18}O$ and δ^2H of these lakes are equivalent to inflow $\delta^{18}O$ and δ^2H, these lakes are assigned E/I values of 0. A small amount of evaporative ^{18}O enrichment may impact measured lake water $\delta^{18}O$ and δ^2H values and true E/I may be marginally greater than 0.

The sensitivity of E/I to primary input parameters (δL, δI, δA, T, and h in the $\delta^{18}O$ formulation) is quantified under Coast/Intermediate, Fjord, and Ice Margin conditions. E/I values are iteratively calculated, varying a single parameter across a range of values representative of uncertainty intervals and interannual variations, with all other parameters held constant at average sub-regional values (Table S2). δL is varied over the range of non-glacial water samples. δI is varied over the average range of maximum monthly precipitation values, which is overlapping and larger than the variation in inferred δI. δA is varied

by 10‰, similar to the range observed in Kangerlussuaq over a 25-day period in summer 2011 (Kopec et al. 2014). Temperature and relative humidity are varied across two standard deviations of ice-free season averages from 1950 to 2018.

Results

Lake water isotopic composition

Measured lake waters exhibit a broad range of isotopic compositions (Fig. 3a). In 2016, $\delta^{18}O$ and $\delta^{2}H$ of 82 non-glacial lake waters ranged from − 17.76 to − 1.54‰ and − 146.45 to − 71.55‰, with median values of − 11.10 ± 3.80‰ and − 104.59 ± 15.40, respectively (uncertainty reported as one standard deviation). d-excess of these samples ranged from − 59.25 to + 4.39‰, with a median of − 19.64 ± 16.45‰. In 2018, $\delta^{18}O$ and $\delta^{2}H$ of 61 non-glacial lake waters varied from − 19.28 to − 8.16‰ and − 142.62 to − 89.64‰, with median values of − 13.22 ± 2.45‰ and − 114.61 ± 15.07, respectively. d-excess of these samples ranged from − 30.17 to + 14.55‰, with a median of 1.02 ± 14.27‰. Comparison of surface and bottom water samples from four non-glacial lakes sampled in 2016 indicates that lakes were well-mixed, with surface waters an average of 0.88‰ ^{18}O and 2.26‰ ^{2}H enriched relative to bottom waters. In 2016, non-glacial lake waters exhibited a strongly significant ($p < 0.01$) trend toward more ^{18}O-enriched values moving inland, though the same trend is not apparent among samples from 2018 (Fig. 4a). In both years, non-glacial lakes demonstrate significant ($p < 0.0001$) decreases in d-excess moving eastward from the coast (Fig. 4b).

Non-glacial lakes sampled in both years exhibit coherent variations (Table S4). Generally, Intermediate sub-region samples from 2018 are slightly ^{18}O-depleted and have higher d-excess relative to samples collected in 2016 from the same lakes (Fig. 3c), with an average offset (2018 minus 2016) of − 0.80‰ for $\delta^{18}O$ and + 3.61‰ for d-excess. Resampled lakes within the Ice Margin sub-region are more strongly ^{18}O-depleted in 2018 relative to 2016, by an average of − 3.70‰, accompanied by an average increase in d-excess of 12.97‰ (Fig. 3d).

$\delta^{18}O$ and $\delta^{2}H$ of proglacial lakes sampled in 2016 (n = 7), ranged from − 31.64 to − 21.13‰ and − 252.49 to − 167.84‰, with median values of − 27.63 ± 3.38‰ and − 218.70 ± 30, respectively (Fig. 3a). Proglacial lake d-excess ranged from − 2.16 to + 4.38‰, with a median of 2.34 ± 2.29‰. Two proglacial lake water samples were collected in 2018, with $\delta^{18}O$ and $\delta^{2}H$ values of − 26.89‰ and − 27.92‰, and − 207.23 and − 217.77, and d-excess of 7.90‰ and 5.60‰, respectively. Surface waters of proglacial lakes were on average 0.68‰ ^{18}O- and 0.98‰ ^{2}H-enriched relative to bottom waters, based on four proglacial lakes sampled in 2016. The lower bound of proglacial lake $\delta^{18}O$ is consistent with values in ice cores retrieved from the ice sheet margin near Kangerlussuaq, which record mean $\delta^{18}O$ values of approximately − 28‰ and − 34‰ for ice dated to the early Holocene and Last Glacial Maximum, respectively (Reeh et al. 2002). The upper bound of proglacial lake $\delta^{18}O$ variation overlaps with snowpack samples collected near the ice margin (Lindborg et al. 2016). Proglacial lake $\delta^{18}O$ measured in both years exhibits a steep trend towards ^{18}O depletion with decreasing distance from the ice margin (Fig. 4a). Proglacial lake d-excess, however, demonstrates no correlation with longitude, varying by less than 5‰ around the median (Fig. 4b). The westward increase in proglacial lake water $\delta^{18}O$, with little change in d-excess, reflects a progressive decrease in the fraction of inflow sourced from ice sheet meltwater relative to precipitation, with little influence of evaporation because of high throughflow. Hereafter, we focus on non-glacial lake waters for their relevance to inferring past precipitation isotope values and P-E.

Inferred inflow $\delta^{18}O$

Applying the conventional LEL-MWL intersection method for estimating source water $\delta^{18}O$ yields average values of − 17.15‰ (2016) and − 17.83‰ (2018) for all non-glacial lakes. Calculation based on sub-regional LELs resolves progressive ^{18}O depletion moving inland, by 10.10‰ (2016) and 6.05‰ (2018) (Fig. 3b–d, Table S3). Bayesian inflow modeling yields similar values, while highlighting the potential for significant variation at finer spatial resolution. δI ranged from − 23.0 to − 11.8‰ in 2016, and − 22.9 to − 12.4‰ in 2018, with similar median values of

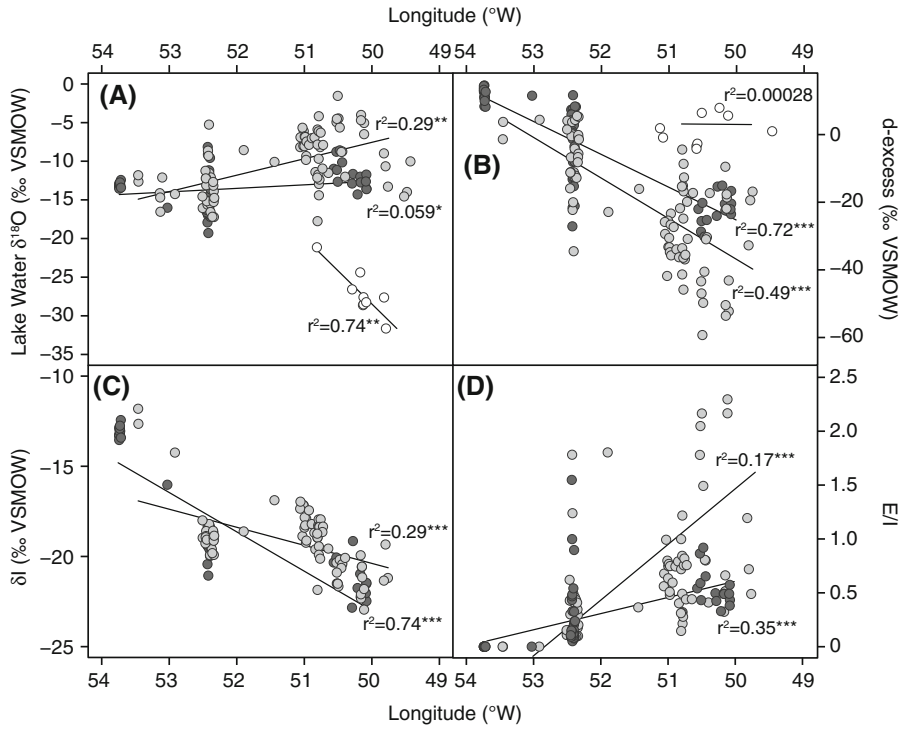

Fig. 4 Spatial trends in measured and inferred parameters for non-glacial lakes in 2016 (light gray), non-glacial lakes in 2018 (dark gray), and proglacial lakes (2016 and 2018, white). **a** Longitude versus measured $\delta^{18}O$. **b** Longitude versus d-excess. **c** Longitude versus δI. **d** Longitude versus evaporation to inflow ratio (E/I). Values less than 0 and greater than 2.5 are cropped from plot, but included in linear regression calculation. Asterisks indicate levels of significance determined from *p* values, where: $*p < 0.05$; $**p < 0.01$; $***p < 0.001$

− 18.0 ± 1.8‰ (2016) and − 19.2 ± 3.1‰ (2018) (Figs. 4c, 5). 90% confidence intervals on δI range from ± 1.8 to 5.3‰, averaging ± 3.3‰. δI decreased significantly moving inland ($p < 0.001$) for 2016 and 2018, and no significant changes were modeled in δI for lakes sampled in both years (Fig. 4C, Table S4).

Measurements of channelized inflow $\delta^{18}O$ from three lakes agree with inferred values. For one Coast sub-region lake, where inflow is assumed equivalent to lake water, measured lake water $\delta^{18}O$ (− 13.4 ± 0.1‰) was similar to the values of the major (− 13.0 ± 0.1‰) and secondary inflows (− 13.3 ± 0.1‰) in 2018. Measured channelized

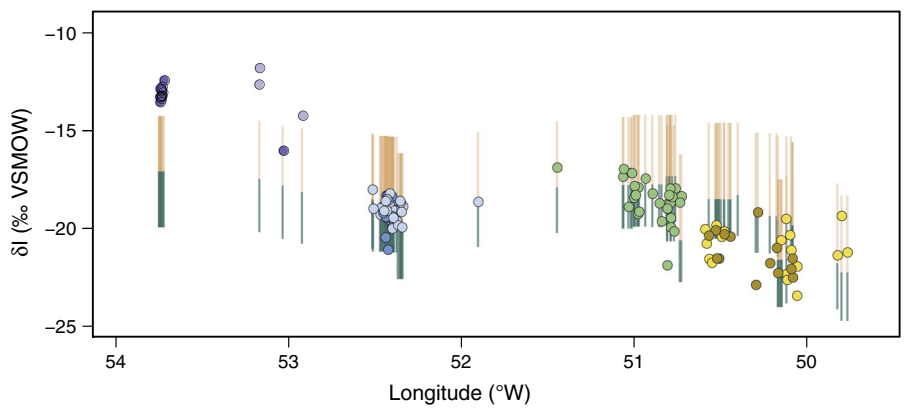

Fig. 5 Comparison of δI of all non-glacial lakes along the longitudinal transect (colors as in Fig. 1) and modeled weighted mean annual and monthly ranges in precipitation $\delta^{18}O$ from the Online Isotopes in Precipitation Calculator (OIPC; Bowen 2018). Yellow and blue bars represent the range between weighted mean annual and maximum and minimum monthly precipitation $\delta^{18}O$ retrieved for each lake coordinate. The grid resolution of OIPC is 5 arc-minutes, reflected in the stepwise changes of modeled precipitation $\delta^{18}O$. (Color figure online)

inflow values from two lakes in the Intermediate sub-region fall within uncertainty ranges of modeled inflow, but as instantaneous samples, were summer-biased in comparison to modeled inflow values, which represent the average value for water retained in the lake basin. For the first lake with measured δL of − 17.0 ± 0.1‰, inflow was modeled as − 19.3 ± 2.4‰ in comparison to measured July inflow of − 17.3 ± 0.1‰ in July 2018. For the second lake with measured δL of − 16.6 ± 0.1‰, inflow was modeled as $\delta^{18}O$ of − 19.2 ± 2.7‰ in comparison to measured July inflow of − 16.5 ± 0.1‰. Most δI estimates fall within the mean annual range of average monthly precipitation $\delta^{18}O$ from the OIPC (Bowen 2018) (Fig. 5). We note, however, that this precipitation range does not capture interannual or sub-monthly variations in precipitation $\delta^{18}O$, and may underestimate variability of precipitation $\delta^{18}O$ on timescales relevant to δI.

Evaporation to inflow ratios

We calculated median E/I values of 0.50 ± 0.32 for 2016 and 0.15 ± 0.28 for 2018 (Fig. 6). E/I increased significantly with longitude in both years ($p < 0.001$) (Fig. 4d). Several (n = 15) lakes, concentrated in the Fjord sub-region, yielded E/I values greater than 1.0, indicating desiccating conditions. For lakes sampled in both years, lower or consistent E/I was observed in 2018 compared to 2016 (Table S4). For resampled lakes in the Ice Margin sub-region, calculated E/I values were lower by an average of − 0.77 in 2018 relative to 2016. In 2016, E/I > 1 indicated desiccating conditions for three of these lakes. In 2018, no lakes were desiccating, with values between 0.59 and 0.92. Resampled lakes in the Intermediate sub-region displayed smaller changes in E/I between years, with values reduced by an average of − 0.06 in 2018 relative to 2016.

One lake sampled in 2016 with exceptionally low d-excess yielded negative E/I, indicating that the observed lake water was more enriched than the modeled limiting lake water isotopic composition, which in turn suggests that the parameters in this model do not adequately characterize this strongly evapo-concentrated lake. Field observations are consistent with the interpretation of these lakes as being in non-steady state, given the presence of lowered shorelines, on seasonal and longer timescales (Aebly and Fritz 2009; Law et al. 2018).

E/I ranged by more than 0.6 for lakes with similar measured $\delta^{18}O$, with scatter driven by variations in both δI and climatological variables (Fig. S3A). Among lakes from the same sub-region, and therefore modeled with the same climatological inputs, E/I of lakes with similar δL varied by approximately 0.3, solely in response to differences in δI. This scatter was reduced when controlling for the influence of variable δI (Fig. S3B).

Testing the sensitivity of E/I to changes in δL illustrates the non-linear relationship between the two variables (Fig. 7a). Large increases in E/I result from substantial increases of δL, as expected. Yet, E/I is relatively insensitive to small positive changes

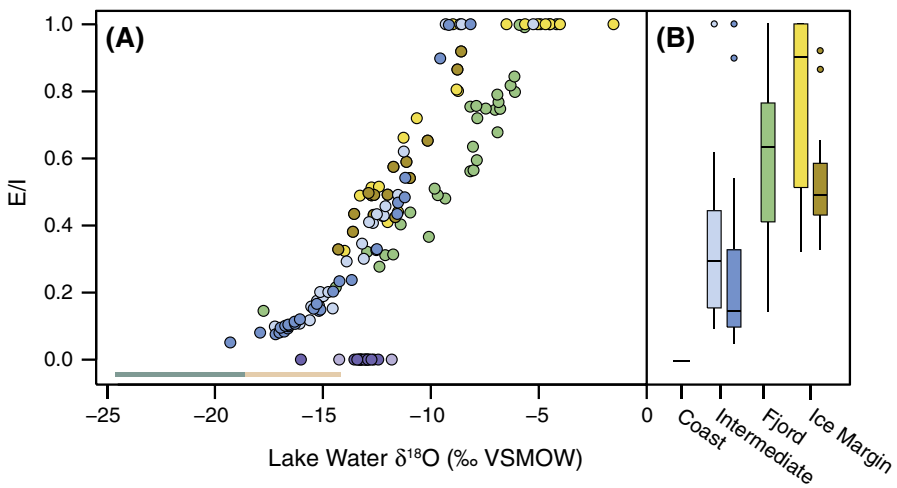

Fig. 6 Evaporation to inflow (E/I) ratios (colors as in Fig. 1). In all panels, E/I ratios less than 0 or greater than 1 are assigned a value of 1. **a** Measured lake water $\delta^{18}O$ versus modeled evaporation to inflow (E/I) with average modeled monthly range in precipitation $\delta^{18}O$ for all lakes denoted by horizontal bar, with colors as in Fig. 5, **b** Boxplots of E/I values divided by sub-region and year

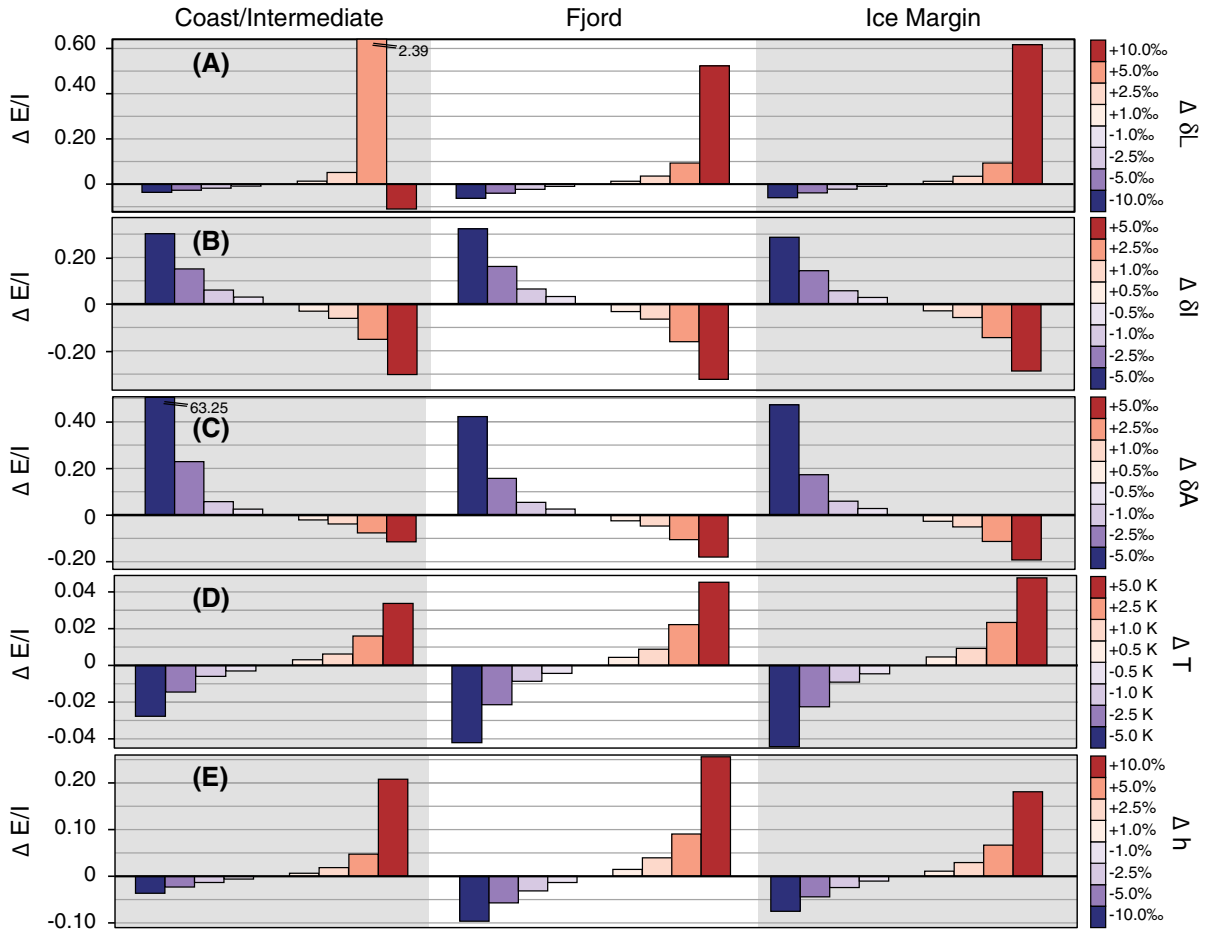

Fig. 7 Sensitivity tests for evaporation to inflow ratios (E/I) for Coast/Intermediate, Fjord, and Ice Margin settings. The height of the bars indicates the magnitude of change on calculated E/I for each parameter as varied by the increments indicated by the key on the right, with all other parameters constant

(< 5‰) and large negative changes (up to − 10‰) in δL. The Coast/Intermediate sub-region demonstrates the smallest variations in E/I of < 0.10 for ΔδL of 2.5‰ and less, including values 10‰ lower than baseline. However, E/I increased by + 2.39 at ΔδL = + 5‰ and decreased by − 0.11 at ΔδL = + 10‰, demonstrating threshold behavior as δL approaches and surpasses the modeled limiting isotopic composition.

Sensitivity testing demonstrates the importance of appropriately characterizing input isotope values for accurate calculation of E/I. Variations in δI produce approximately equivalent and symmetric changes for each sub-region (Fig. 7b). Deviations of ± 5‰ in δI result in E/I variations of ± 0.30, with lower δI resulting in higher E/I. E/I exhibits a strong asymmetric sensitivity to δA among sub-regions, with underestimation of δA by − 5‰ driving increases of E/I greater than 0.40 in all sub-regions (Fig. 7c). E/I results are relatively insensitive to changes in temperature employed in the calculation of fractionation factors, with variation over a range representative of interannual variation in summer temperatures (± 5 K) producing changes in E/I of less than ± 0.05 (Fig. 7d). Relative humidity exerts a slightly stronger control, with increases in relative humidity of up to 10% driving changes in E/I of up to 0.25 (Fig. 7e).

E/I values demonstrate minor offsets when calculated from δ^2H rather than $\delta^{18}O$, which become larger at higher E/I, indicating additional uncertainty in these calculations that is not addressed by these sensitivity tests (Fig. S4). These differences may stem from

uncertainties in δI or δA given poor constraint of the LMWL, as physically, E/I must be equivalent (Yi et al. 2008). Spatial trends in E/I, however, and the relative variability between E/I and δI do not differ substantially between the two estimations. Thus, these particular uncertainties in E/I values do not alter our interpretations.

Discussion

We assessed the sensitivity of modern western Greenland lake water $\delta^{18}O$ to variability in inflow isotope composition and evaporation, analogous to variability in paleo-proxy interpretations of precipitation isotopes and P-E. To resolve the sensitivity of lake water $\delta^{18}O$ and $\delta^{2}H$ to these two controls along an aridity gradient, we quantified variability in δI and E/I. Results of this modeling support the following conclusions, hereafter discussed in greater detail: (1) Regional-scale lake water isotope variability may be broadly classified as inflow- or evaporation-sensitive, (2) both δI and E/I vary in response to regional P-E, indicating persistent influence despite dominant inflow- or evaporation-sensitive patterns, (3) catchment hydrology drives local variability in δI and E/I sensitivity, and (4) proximal, but hydrologically distinct lakes may yield complementary paleoclimate records that are dominantly inflow- or evaporation-sensitive.

Inflow- and evaporation-sensitive variability

Two modes of variation in $\delta^{18}O$–$\delta^{2}H$ space characterize lake water isotopes across our study area, reflecting patterns associated with changes in inflow or evaporation. 'Inflow-sensitive' lake water isotope values vary parallel to MWLs in $\delta^{2}H$-$\delta^{18}O$ space, exhibiting changes in $\delta^{18}O$ independent of changes in d-excess, with no evidence for evapo-concentration (Fig. 3). Conceptually, isotopic variations in 'inflow-sensitive' lake waters are primarily determined by lake water residence time, which determines the time frame over which precipitation-derived inflow is integrated (Jonsson et al. 2009). A second subset of lakes is characterized by ^{18}O enrichment associated with strongly declining d-excess, plotting off MWLs along LELs in $\delta^{2}H$-$\delta^{18}O$ space. We refer to these lakes as 'evaporation-sensitive,' specifically when ^{18}O enrichment and d-excess decreases exceed the magnitude of seasonal variability in precipitation $\delta^{18}O$ and d-excess, implicating modification of lake waters by evaporation. This threshold corresponds to an E/I of approximately 0.5 and coincides with the geographic boundary between positive and negative P-E (Figs. 2, S4B, S4C). Generally, Coast and Intermediate sub-region lakes exhibit inflow-sensitivity, and Fjord and Ice Margin sub-region lakes exhibit evaporation-sensitivity. Although there is an apparent threshold between inflow- and evaporation-sensitive behavior, trends in δI and E/I impact lakes across the study area, indicating persistent influence of both in all lakes.

Regional-scale patterns in inflow and evaporation determined by P-E

Deconvolving variability in lake water isotopes caused by δI and E/I across our study area enables determination of the impacts of δI and E/I on lakes for which they are not the dominant controls. Trends in δI span the entire study area (Fig. 4c), indicating that δI variations influence lake water isotope values even where these signals are overprinted by evaporative ^{18}O enrichment. For both sampling years, δI declined by approximately 11‰ between the coast and ice margin (Fig. 5). Eastward depletion of δI may reflect progressive Rayleigh Distillation during inland moisture transport (Dansgaard 1964). OIPC-modeled amount-weighted mean annual precipitation $\delta^{18}O$ (δP), however, declines by only 5.1‰ across the same transect (Fig. 5) (Bowen 2018). The discrepancy in the ranges of δI and mean annual δP suggests that δI variations are the result of catchment-scale hydrological processes rather than differences in mean annual δP values.

Biases in the seasonality of precipitation integrated by lake waters may exaggerate the longitudinal trend in δI relative to δP. Comparison of δI to δP suggests a shifting tendency from summer-biased inflow at the coast to winter-biased inflow inland (Fig. 5). δI of Coast sub-region lakes falls within or above the range of summer δP, whereas δI of Intermediate sub-region lakes approximates mean annual δP, and δI falls within the range of winter δP for most Fjord and Ice Margin sub-region lakes. The observed regional-scale trend in inflow seasonality is likely a response to the seasonality of the aridity gradient (Fig. 2). Although all lakes within the study area likely experience

efficient recharge by snowpack melt in spring, inland lakes may receive a smaller fraction of summer precipitation because of lower relative humidity and higher catchment evapotranspiration (Bowen et al. 2018). The resulting winter bias in inland lake water isotope compositions occurs despite a greater fraction of annual precipitation falling during the summer months in these regions. The precipitation seasonality represented by δI is determined by seasonal P-E balance, rather than seasonal precipitation amount alone.

E/I increases significantly between the coast and ice margin, associated with ^{18}O enrichments in δL from 0 to 19.97‰ (Fig. 4d, S3B). This trend is consistent with the strong difference in ice-free-season relative humidity between the Coast and Fjord/Ice Margin sub-regions, and may be exaggerated by seasonal temperature differences (Fig. 2). Earliest ice melt in western Greenland is typically observed near the head of Kangerlussuaq Fjord in mid-June, whereas relatively cool coastal summers promote the persistence of fog banks, reducing radiation and substantially delaying ice-out in coastal lakes by multiple weeks (Anderson and Brodersen 2001). Therefore, inland sites are biased towards a longer duration of evaporation, which, coupled with lower relative humidity, results in enhanced evaporative ^{18}O enrichment relative to coastal lakes.

Local variability in δI and E/I determined by catchment hydrology

In addition to trends spanning the entire study area, δI varied by an average of 4.0‰ among lakes of the same sub-region (Fig. 5). Catchment-scale variations in δI are likely controlled by residence time, a function of lake basin volume and inflow volume, dependent on catchment area and precipitation amount (Jonsson et al. 2009). Small lakes with higher throughflow and shorter residence times will reflect short-term precipitation seasonality closely, whereas larger lakes with low throughflow and long residence time integrate longer-term precipitation seasonality (Gibson et al. 2002; Leng and Anderson 2003). Other factors contributing to local variations in δI include hydrologic connectivity between lakes and their surrounding catchments. For example, in low-relief catchments, meltwater may form patchy vernal pools that may refreeze temporarily until the uppermost soil thaws, reducing or delaying snowmelt delivery to lakes (Johansson et al. 2015; Lindborg et al. 2016).

Intermediate, Fjord, and Ice Margin sub-regions all include lakes with variable E/I ranging from < 0.5 to > 1.0 (Fig. 6). Within these sub-regions, ^{18}O enrichment relative to δI (ΔδL) ranges by an average of 8.96‰. A maximum range of ΔδL is observed among sampled Ice Margin sub-region lakes, from 5.94 to 19.97‰. As with δI, residence time is likely a primary control on local variations in ΔδL and E/I. Lakes with short residence times will flush faster than the build-up of evaporative signals, whereas lakes with comparatively long residence times may develop signals of ^{18}O enrichment over months to years. The sensitivity of a lake to the development of interannual evaporative signals is likely controlled by the efficacy with which spring melt flushes lake waters, which depends on the magnitude of snowmelt inflow relative to lake volume. Leng and Anderson (2003) hypothesized that small lakes with relatively large catchments are most likely to be 'reset' by snowmelt each spring, receiving the greatest flux of spring melt relative to lake volume. Because significantly more winter precipitation falls at the coast than inland, Coast sub-region lakes are more likely to be fully 'reset' during the spring melt period than are inland lakes (Fig. 2e). Seasonal inflow amount thus modulates sensitivity to E/I in lakes with residence times longer than a single ice-free season. Hence, variations in inflow amount, and by extension isotopic composition, underlie evaporation-sensitive lake waters, despite emerging only as the dominant control when not overprinted by evaporation.

Implications for paleoclimate studies

Although interpretation of a lake water isotope proxy record in terms of either P-E (E/I) or precipitation isotopes (δI) is standard, a major assumption is that the primary control on δL (and sensitivity to the control) remained consistent over the length of the record. Here, spatial patterns of δI and E/I in lakes across a modern aridity gradient illustrate that lake water sensitivity to isotopic controls fluctuates in response to hydroclimate, implying that controls on hydroclimate-sensitive paleo-records may vary in response to the same hydroclimate changes that they aim to infer.

δI and E/I are both affected by residence time and therefore precipitation amount, and care must be taken to distinguish these effects in paleoclimate

interpretations. For example, given a predominantly inflow-sensitive record, an increase in precipitation would decrease the residence time of a lake, changing the representative seasonality of precipitation isotopes sampled by a proxy from the lake water. Alternatively, given a predominantly evaporation-sensitive lake, an increase in precipitation amount may decrease the retention of interannual ^{18}O-enrichment signals, increasing the relative sensitivity to inflow variations. Caution should be taken to not interpret these changes as small-scale P-E variations.

Even so, it may be possible to constrain past combined variations in evaporation and inflow. The use of proxy system models with a range of complexity will be key in moving beyond the interpretation of relative trends from lake water isotope proxy records (Dee et al. 2018; Morrill et al. 2019). For example, a simple proxy system model of lake water residence time may yield constraints on impacts of δI and E/I on an individual lake record. Given lake volume, catchment area, and monthly total precipitation and δP, calculation of a lake's residence time enables approximation of δI under modern climate conditions and a first-order assessment of the lake system to reproduce reasonable paleoclimate data. Complex proxy system models such as PRYSM2.0 may incorporate modern climate data or paleoclimate model output, enabling sensitivity testing to determine which parameters most likely caused reconstructed isotope variations (Dee et al. 2018). Time slices from isotope-enabled climate models such as the GISS ModelE-R and ECHAM5 (Schmidt et al. 2007; Werner et al. 2011) may provide parameters required for isotope mass balance calculations for periods that lack observational data, enabling quantification of the relative magnitude of isotopic changes expected from E/I relative to δI, and quantitative estimates of E/I.

Proxy system model-based sensitivity testing may enable the identification of hydrologically distinct lakes within a region that demonstrate end-member evaporation-sensitive and inflow-sensitive isotopic variability. E/I varies from near 0 to > 1 within the Intermediate and Fjord sub-regions, demonstrating the potential for strong differences in hydrologic sensitivity within a small region (Fig. 6). Downcore data from these end-member lakes may yield hydroclimate records that are comparatively evaporation- and inflow-sensitive. Furthermore, provided that variations in δI primarily reflect variations in the integration of seasonal δP, lakes with contrasting residence times in regions of high P-E may yield seasonally specific precipitation isotope records (i.e. summer precipitation vs. mean annual precipitation). Two windows of integration must be considered in the interpretation of inflow-sensitive paleoclimate records: the integration of precipitation isotopes in lake water and the integration of lake water in the proxy, and thus the representative precipitation isotope seasonality may differ from the seasonality of proxy growth. Among the minimally evapo-concentrated lakes of the Coast and Intermediate sub-regions, δI for samples taken in the summer ranged from -21.86 to -11.81‰, comparable to the range in modeled monthly δP. Therefore, lakes with different residence times within the same region may be targeted to provide downcore records with differing precipitation isotope seasonality, even if the seasonality of proxy growth is the same in both systems. Such resolved records are necessary to constrain paleo-variability of the seasonal mechanisms driving projected changes in the Arctic hydrological cycle.

Acknowledgements Data may be accessed in the supplementary file and at waterisotopes.org (Project ID 00256). This research was supported by the NSF ARCSS-1504267 Snow on Ice Project and an NSF Graduate Research Fellowship to A.A.C. We thank David H. Boutt for instrumental analysis of 2016 water samples, Kayla Hollister and Owen Cowling for lab assistance, Jason Briner, Megan Corcoran, Josh Cuzzone, Brandon Graham, Kayla Hollister, Anna McKee, Alia Lesnek, Heidi Roop, Margie Turrin, and Nicolás Young for assistance with sampling, and CH2M Hill Polar Services for logistical support. Meteorological data were provided by the Danish Meteorological Organization and the Programme for Monitoring of the Greenland Ice Sheet (PROMICE), by the Geological Survey of Denmark and Greenland (GEUS), and the National Center for Environmental Information (NCEI).

Compliance with ethical standards

Conflict of interest The authors declare no financial conflicts of interests

References

Aebly FA, Fritz SC (2009) Palaeohydrology of Kangerlussuaq (Søndre Strømfjord), West Greenland during the last ~8000 years. Holocene 19:91–104. https://doi.org/10.1177/0959683608096601

Andersen KK, Azuma N, Barnola JM et al (2004) High-resolution record of Northern Hemisphere climate extending

into the last interglacial period. Nature 431:147–151. https://doi.org/10.1038/nature02805

Anderson NJ, Brodersen KP (2001) Determining the date of ice-melt for low Arctic lakes along Søndre Strømfjord, southern West Greenland. Geol Greenl Surv Bull 189:54–58

Anderson NJ, Leng MJ (2004) Increased aridity during the early Holocene in West Greenland inferred from stable isotopes in laminated-lake sediments. Quat Sci Rev 23:841–849. https://doi.org/10.1016/j.quascirev.2003.06.013

Anderson NJ, Bennike O, Christoffersen K et al (1999) Limnological and palaeolimnological studies of lakes in southwestern Greenland. Geol Greenl Surv Bull 183:68–74

Anderson L, Abbott MB, Finney BP, Burns SJ (2005) Regional atmospheric circulation change in the North Pacific during the Holocene inferred from lacustrine carbonate oxygen isotopes, Yukon Territory, Canada. Quat Res 64:21–35. https://doi.org/10.1016/j.yqres.2005.03.005

Arppe L, Kurki E, Wooller MJ et al (2017) A 5500-year oxygen isotope record of high arctic environmental change from southern Spitsbergen. Holocene 27:1948–1962. https://doi.org/10.1177/0959683617715698

Balascio NL, D'Andrea WJ, Bradley RS, Perren BB (2013) Biogeochemical evidence for hydrologic changes during the Holocene in a lake sediment record from southeast Greenland. Holocene 23:1428–1439. https://doi.org/10.1177/0959683613493938

Balascio NL, D'Andrea WJ, Gjerde M, Bakke J (2018) Hydroclimate variability of High Arctic Svalbard during the Holocene inferred from hydrogen isotopes of leaf waxes. Quat Sci Rev 183:177–187. https://doi.org/10.1016/j.quascirev.2016.11.036

Bintanja R, Selten FM (2014) Future increases in Arctic precipitation linked to local evaporation and sea-ice retreat. Nature 509:479. https://doi.org/10.1038/nature13259

Bowen GJ (2018) The Online Isotopes in Precipitation Calculator version 3.1. http://www.waterisotopes.org. Accessed 2 Apr 2018

Bowen GJ, Putman A, Brooks JR, Bowling DR, Oerter EJ, Good SP (2018) Inferring the source of evaporated waters using stable H and O isotopes. Oecologia 187:1025–1039. https://doi.org/10.1007/s00442-018-4192-5

Bring A, Fedorova I, Dibike Y et al (2016) Arctic terrestrial hydrology: a synthesis of processes, regional effects, and research challenges. J Geophys Res Biogeosci 121:621–649. https://doi.org/10.1002/2015JG003131

Bush RT, Berke MA, Jacobson AD (2017) Plant water δD and δ18O of tundra species from West Greenland. Arct Antarct Alp Res 49:341–358. https://doi.org/10.1657/AAAR0016-025

Cappelen J (2017) Weather observations from Greenland 1958-2016. DMI Technical Report 17-08

Clark ID, Fritz P (1997) Environmental isotopes in hydrogeology. CRC Press, Cambridge

Craig H (1961) Isotopic variations in meteoric waters. Science 133:1702–1703. https://doi.org/10.1126/science.133.3465.1702

Craig H, Gordon LI (1965) Deuterium and oxygen 18 variations in the ocean and the marine atmosphere. In: Tongiorgi E (ed) Stable isotopes in oceanographic studies and paleotemperatures. Consiglio nazionale delle ricerche, Pisa, Italy, Spoleto: Conferences in Nuclear Geology, pp 9–130

Dansgaard W (1964) Stable isotopes in precipitation. Tellus 16:436–468. https://doi.org/10.3402/tellusa.v16i4.8993

Dansgaard W, Johnsen SJ, Clausen HB et al (1993) Evidence for general instability of past climate from a 250-kyr ice-core record. Nature 364:218–220. https://doi.org/10.1038/364218a0

Dee SG, Russell JM, Morrill C et al (2018) PRYSM v2.0: a proxy system model for lacustrine archives. Paleoceanogr Paleocl 33:1250–1269. https://doi.org/10.1029/2018PA003413

Feng X, Lauder AM, Posmentier ES et al (2016) Evaporation and transport of water isotopologues from Greenland lakes: the lake size effect. Quat Sci Rev 131:302–315. https://doi.org/10.1016/j.quascirev.2015.07.029

Gat JR (1995) Stable isotopes of fresh and saline lakes. In: Lerman A, Imboden DM, Gat JR (eds) Physics and chemistry of lakes. Springer, Berlin, pp 139–165

Gat JR (1996) Oxygen and hydrogen isotopes in the hydrologic cycle. Annu Rev Earth Planet Sci 24:225–262. https://doi.org/10.1146/annurev.earth.24.1.225

Gat JR (2000) Atmospheric water balance—the isotopic perspective. Hydrol Process 14:1357–1369. https://doi.org/10.1002/1099-1085(20000615)14:8%3c1357:AID-HYP986%3e3.0.CO;2-7

Gibson JJ (2002) Short-term evaporation and water budget comparisons in shallow Arctic lakes using non-steady isotope mass balance. J Hydrol 264:242–261. https://doi.org/10.1016/S0022-1694(02)00091-4

Gibson JJ, Edwards TWD (2002) Regional water balance trends and evaporation-transpiration partitioning from a stable isotope survey of lakes in northern Canada. Global Biogeochem Cycles 16:10–11. https://doi.org/10.1029/2001GB001839

Gibson JJ, Prepas EE, McEachern P (2002) Quantitative comparison of lake throughflow, residency, and catchment runoff using stable isotopes: modelling and results from a regional survey of Boreal lakes. J Hydrol 262:128–144. https://doi.org/10.1016/S0022-1694(02)00022-7

Gibson JJ, Birks SJ, Edwards TWD (2008) Global prediction of δA and δ^2H-$\delta^{18}O$ evaporation slopes for lakes and soil water accounting for seasonality. Global Biogeochem Cycles. https://doi.org/10.1029/2007GB002997

Gibson JJ, Birks SJ, Yi Y (2016) Stable isotope mass balance of lakes: a contemporary perspective. Quat Sci Rev 131:316–328. https://doi.org/10.1016/j.quascirev.2015.04.013

Gonfiantini R (1986) Environmental isotopes in lake studies. In: Fritz P, Fontes JC (eds) Handbook of environmental isotope geochemistry: the terrestrial environment. Elsevier, New York, pp 113–168

Hasholt B, Søgaard H (1978) Et Forsøg på en klimatisk-hydrologisk regionsinddeling af Holsteinsborg Kommune (Sisimiut). Geografisk tidsskrift 77:72–92. https://doi.org/10.1080/00167223.1978.10649095

Henkemans E, Frape SK, Ruskeeniemi T et al (2018) A landscape-isotopic approach to the geochemical

characterization of lakes in the Kangerlussuaq region, west Greenland. Arct Antarct Alp Res. https://doi.org/10.1080/15230430.2017.1420863

Horita J, Wesolowski DJ (1994) Liquid-vapor fractionation of oxygen and hydrogen isotopes of water from the freezing to the critical temperature. Geochim Cosmochim Acta 58: 3425–3437. https://doi.org/10.1016/0016-7037(94)90096-5

Horita J, Rozanski K, Cohen S (2008) Isotope effects in the evaporation of water: a status report of the Craig-Gordon model. Isot Environ Health Stud 44:23–49. https://doi.org/10.1080/10256010801887174

IAEA/WMO (2018) Global network of isotopes in precipitation database. https://www.iaea.org/services/networks/gnip. Accessed 2 Apr 2018

Johansson E, Gustafsson L-G, Berglund S et al (2015) Data evaluation and numerical modeling of hydrological interactions between active layer, lake and talik in a permafrost catchment, Western Greenland. J Hydrol 527:688–703. https://doi.org/10.1016/j.jhydrol.2015.05.026

Jonsson CE, Leng MJ, Rosqvist GC et al (2009) Stable oxygen and hydrogen isotopes in sub-Arctic lake waters from northern Sweden. J Hydrol 376:143–151. https://doi.org/10.1016/j.jhydrol.2009.07.021

Kopec BG, Lauder AM, Posmentier ES, Feng X (2014) The diel cycle of water vapor in west Greenland. J Geophys Res Atmos 119:9386–9399. https://doi.org/10.1002/2014JD021859

Kopec BG, Feng X, Posmentier ES et al (2018) Use of principal component analysis to extract environmental information from lake water isotopic compositions. Limnol Oceanogr 63:1340–1354. https://doi.org/10.1002/lno.10776

Lasher GE, Axford Y (2019) Medieval warmth confirmed at the Norse Eastern Settlement in Greenland. Geology 47:267–270. https://doi.org/10.1130/G45833.1

Lasher GE, Axford Y, McFarlin JM et al (2017) Holocene temperatures and isotopes of precipitation in Northwest Greenland recorded in lacustrine organic materials. Quat Sci Rev 170:45–55. https://doi.org/10.1016/j.quascirev.2017.06.016

Law AC, Nobajas A, Sangonzalo R (2018) Heterogeneous changes in the surface area of lakes in the Kangerlussuaq area of southwestern Greenland between 1995 and 2017. Arct Antarct Alp Res. https://doi.org/10.1080/15230430.2018.1487744

Leng MJ, Anderson NJ (2003) Isotopic variation in modern lake waters from western Greenland. Holocene 13:605–611. https://doi.org/10.1191/0959683603hl620rr

Leng MJ, Marshall JD (2004) Palaeoclimate interpretation of stable isotope data from lake sediment archives. Quat Sci Rev 23:811–831. https://doi.org/10.1016/j.quascirev.2003.06.012

Leng MJ, Wagner B, Anderson NJ et al (2012) Deglaciation and catchment ontogeny in coastal south-west Greenland: implications for terrestrial and aquatic carbon cycling. J Quat Sci 27:575–584. https://doi.org/10.1002/jqs.2544

Lesnek AJ, Briner JP, Young NE, Cuzzone JK (2020) Maximum Southwest Greenland Ice Sheet recession in the early Holocene. Geophys Res Lett. https://doi.org/10.1029/2019GL083164

Lindborg T, Rydberg J, Tröjbom M et al (2016) Biogeochemical data from terrestrial and aquatic ecosystems in a periglacial catchment, West Greenland. Earth Syst Sci Data 8:439. https://doi.org/10.5194/essd-8-439-2016

Linderholm HW, Nicolle M, Francus P et al (2018) Arctic hydroclimate variability during the last 2000 years – current understanding and research challenges. Clim Past 14:473–514. https://doi.org/10.5194/cp-14-473-2018

Morrill C, Meador E, Livneh B et al (2019) Quantitative model-data comparison of mid-Holocene lake-level change in the central Rocky Mountains. Clim Dyn 53:1077–1094. https://doi.org/10.1007/s00382-019-04633-3

NOAA (2018) National Center for Environmental Information Climate Data Online. https://www.ncdc.noaa.gov/data-access/land-based-station-data. Accessed 18 Oct 2018

Rawlins MA, Steele M, Holland MM et al (2010) Analysis of the Arctic system for freshwater cycle intensification: observations and expectations. J Clim 23:5715–5737. https://doi.org/10.1175/2010JCLI3421.1

Reeh N, Oerter H, Thomsen HH (2002) Comparison between Greenland ice-margin and ice-core oxygen-18 records. Ann Glaciol 35:136–144. https://doi.org/10.3189/172756402781817365

Schmidt GA, LeGrande AN, Hoffmann G (2007) Water isotope expressions of intrinsic and forced variability in a coupled ocean-atmosphere model. J Geophys Res Atmos. https://doi.org/10.1029/2006JD007781

Serreze MC, Barrett AP, Slater AG et al (2006) The large-scale freshwater cycle of the Arctic. J Geophys Res-Oceans 111:C11010. https://doi.org/10.1029/2005JC003424

Smeets PCJP, Munneke PK, van As D et al (2018) The K-transect in west Greenland: automatic weather station data (1993–2016). Arct Antarct Alp Res. https://doi.org/10.1080/15230430.2017.1420954

Sundqvist HS, Kaufman DS, McKay NP et al (2014) Arctic Holocene proxy climate database–new approaches to assessing geochronological accuracy and encoding climate variables. Clim Past 10:1605–1631. https://doi.org/10.5194/cp-10-1605-2014

Thomas EK, Briner JP, Ryan-Henry JJ, Huang Y (2016) A major increase in winter snowfall during the middle Holocene on western Greenland caused by reduced sea ice in Baffin Bay and the Labrador Sea. Geophys Res Lett. https://doi.org/10.1002/2016GL068513

Thomas EK, Castañeda IS, McKay NP et al (2018) A wetter Arctic coincident with hemispheric warming 8,000 years ago. Geophys Res Lett 45:10,637–10,647. https://doi.org/10.1029/2018GL079517

van Geldern R, Barth JAC (2012) Optimization of instrument setup and post-run corrections for oxygen and hydrogen stable isotope measurements of water by isotope ratio infrared spectroscopy (IRIS). Limnol Oceanogr Methods 10:1024–1036. https://doi.org/10.4319/lom.2012.10.1024

Van Tatenhove FGM, Olesen OB (1994) Ground temperature and related permafrost characteristics in west greenland. Permafrost Periglac Process 5:199–215. https://doi.org/10.1002/ppp.3430050402

Werner M, Langebroek PM, Carlsen T, Herold M, Lohmann G (2011) Stable water isotopes in the ECHAM5 general circulation model: toward high-resolution isotope modeling

on a global scale. J Geophys Res Atmos. https://doi.org/10.1029/2011JD015681

Yi Y, Brock BE, Falcone MD et al (2008) A coupled isotope tracer method to characterize input water to lakes. J Hydrol 350:1–13. https://doi.org/10.1016/j.jhydrol.2007.11.008